Prediction of Interfacial Debonding in Fiber-Reinforced Composite Laminates

Zhou, Yi; Huang, Zheng-Ming; Liu, Ling

Published in:
Polymer Composites

DOI:
10.1002/pc.24943

Publication date:
2019

Prediction of Interfacial Debonding in Fiber-Reinforced Composite Laminates

Yi Zhou,[1] Zheng-Ming Huang,[1]* Ling Liu[2]
[1]*School of Aerospace Engineering & Applied Mechanics, Key Laboratory of the Ministry of Education for Advanced Civil Engineering Materials, Tongji University, 1239 Siping Road, Shanghai, 200092, China*

[2]*Micromechanics of Materials, Zernike Institute for Advanced Materials, University of Groningen, 9747 AG, Groningen, The Netherlands*

An analytical method is established to estimate the load level when interfacial debonding occurs between fibers and matrix of a composite under an arbitrary load. Only the transverse tensile strength and the components' properties of the unidirectional (UD) composite are required for this estimation. For internal stress analysis based on micromechanics, the homogenized stresses in matrix must be converted into true values because of the nonuniform stress distribution due to embedded fiber. The stress concentration factors (SCFs) of matrix before and after the interfacial debonding are both essential, between which the difference indicates the effect of debonding on the stress fluctuations in matrix. A final true stress is obtained by accumulating the products of stress increments of matrix arising before and after debonding and corresponding SCFs. Letting the predicted transverse tensile strength of a UD composite with an initial perfect and later cracked interface be equal to the measured corresponding value, a critical von Mises stress of matrix at which the interfacial cracks appear is obtained. For a UD composite subjected to an arbitrary load, when the principal stress is positive and the von Mises stress of matrix reaches the critical value, the applied load level when interfacial debonding occurs is determined accordingly. POLYM. COMPOS., 40:1828–1841, 2019. © 2018 Society of Plastics Engineers

INTRODUCTION

The fiber/matrix interface of composites plays a key role in loading transferring between constituent materials. To improve the overall load carrying capacity of composites, a great many techniques have been developed to carry out interface modifications, including liquid [1] and gas [2] phase oxidations, coupling agent sizing [3], polymer coating [4], ultrasonic [5], and irradiation [6] treatments. Nevertheless, given a fiber and matrix system, it is still a challenge to judge whether the interface between the two components is strong enough under a certain loading condition and how much potential improvement can be achieved through interface modification. Efforts have been made to characterize the interfacial strength of composites for a long time [7]. So far, the most common ways are still tests based on single fiber or fiber tow microcomposites [8], such as the fiber fragmentation test [9], fiber pull-out test [10], micro-drop technique [11], and cruciform (or cross-shaped) specimen transverse tension experiment [12]. Due to difference in dimension, the measuring objects used in these tests are always different with an actual composite on the aspects of mechanical and physical–chemical conditions. Furthermore, manufacturing and testing these microcomposite specimens are not easy for practice engineers. So far, there is no experimental standard for these microscopic tests to follow, thus a wide dispersion exists among results obtained from repeat tests done by different testers. Overall, measurements obtained from these methods are not ideal to be directly used for predicting the mechanical properties of composites [[8,11,13].

On the other hand, many works have also been done to characterize the interfacial strength by measuring the macroscopic mechanical behavior of a composite. [±45]s laminates tension test, Iosipescu shear test, short-beam shear test are most frequently used. Madhukar and Drzal [14] compared the interfacial strengths of a material system given by different measuring methods, including the three macroscopic shearing tests and several microscopic tests, finding that there were large discrepancies among results obtained from these methods. They also pointed out that none of these macroscopic shearing tests could characterize interfacial properties accurately. As explained in Ref. [15], a macroscopic test could only characterize the interfacial strength qualitatively because the inside broken part of a composite was difficult to observe clearly and complex failure modes would influence the experimental

Correspondence to: Z.-M. Huang; e-mail: huangzm@tongji.edu.cn
Contract grant sponsor: National Natural Science Foundation of China; contract grant numbers: 11832014, 11472192.
DOI 10.1002/pc.24943
Published online in Wiley Online Library (wileyonlinelibrary.com).

result. Therefore, it is hard to deduce accurate microscopic interfacial properties from macroscopic measuring data.

Other works relying on computational simulations tend to build models with assumed interfacial strengths and compare the simulated mechanical properties with the measurements to judge if the assumed properties are reasonable. Blackketter et al. [16] developed a finite element model (FEM) to determine an interfacial strength by comparing the analog value of the transverse flexural strength of a composite with the corresponding measurement. Sun et al. [17] used a method of cells to retrieve interfacial strengths from off-axial tensile tests. Two off-axial tensile strengths of a composite with different off-axial angles were needed to determine the ratio of the interfacial tensile and shear strengths, which is necessary for the application of Hashin's failure criterion. Hobbiebrunken et al. [18] used FEM to estimate the interfacial strengths of a laminate from three-point bending tests with a pre-assumption that the maximum normal and shear stresses on the interface when interfacial debonding occurs could be regarded as the interfacial normal and shear strengths, respectively. They admitted that the interfacial shear strength obtained in this way was inaccurate [18]. Qi et al. [19] used a generalized method of cells with the maximum stress failure criterion to estimate the interfacial tensile strength based on transverse fiber bundle tension test. The interfacial moduli were assumed to follow a power law variation along the radial direction. Thus it can be seen, there are various preassumptions about interfacial properties among these models without a credible standard.

The purpose of this study is to estimate the load level when interfacial debonding occurs and the failure strength of a composite with an initial perfect and later cracked interface subjected to an arbitrary load, with only the components' properties and the transverse tensile strength in hand. When predict the mechanical behavior of a composite based on a micromechanical model, the homogenized stresses in the matrix must be converted to true values in terms of the stress concentration factors (SCFs). In other words, each volume-averaged matrix stress component calculated through a micromechanical model must be multiplied by a corresponding SCF before failure analysis [20,21]. Such an SCF cannot be defined in a classical way by dividing the maximum point stress by the surface-averaged stress. It must be determined based on an averaged quantity instead. The SCFs of the matrix in a composite subjected to transverse tension, transverse compression, and transverse shear respectively have been derived based on an assumption of perfect interfacial bonding [20,21]. In this article, a new longitudinal shear SCF is derived. More importantly, the transverse tensile SCF of composites with interfacial cracks is put forward. While it is widely accepted that bad interfacial adhesion tends to weaken the ultimate strength of composites because interfacial cracks hinder effective loading transferring between matrix and fibers, few attention is given to the effect of interfacial debonding on stress fluctuations in matrix, which is reflected by the SCFs in this paper. To determine the load level at the moment interfacial debonding occurs, the predicted transverse tensile strength of a UD composite with an initial perfect and later cracked interface is assumed to be equal to the measured counterpart, with a critical von Mises stress of matrix determined accordingly. The composite subjected to any other load is expected to undergo interfacial cracks initiation if the current von Mises stress in the matrix is equal to or greater than the critical value. Different from other works about the interfacial debonding problems, no specific microscopic interfacial strength parameter is employed in this theory. Instead, there is only one intuitive macroscopic mechanical property of a composite, the transverse tensile strength, is related directly, thus errors due to transformation of scales can be avoided. To illustrate our theory, two UD composites are chosen as examples with their components' properties and transverse tensile strengths given as known conditions. The interfacial cracks initiations and ultimate strengths of the two composites under off-axial tension with different off-axial angles are estimated, respectively, and compared with measurements.

INTERNAL STRESS DETERMINATION

The homogenized stresses in fibers and matrix of a composite have relationship below:

$$\{\sigma_i\} = V_{\mathrm{f}}\{\sigma_i^{\mathrm{f}}\} + V_{\mathrm{m}}\{\sigma_i^{\mathrm{m}}\}, \tag{1}$$

where V is the volume fraction, with subscript f or m referring to fiber or matrix, respectively. Connecting the homogenized stresses in component materials with a bridging tensor, $[A_{ij}]$, one has

$$\{\sigma_i^{\mathrm{m}}\} = [A_{ij}]\{\sigma_j^{\mathrm{f}}\}. \tag{2}$$

Equations 1 and 2 lead to

$$\{\sigma_i^{\mathrm{f}}\} = (V_{\mathrm{f}}[I] + V_{\mathrm{m}}[A_{ij}])^{-1}\{\sigma_j\} = [B_{ij}]\{\sigma_j\}, \tag{3}$$

$$\{\sigma_i^{\mathrm{m}}\} = [A_{ij}][B_{ij}]\{\sigma_j\}. \tag{4}$$

Further, the compliance tensor of the composite is given by [22]

$$[S_{ij}] = (V_{\mathrm{f}}[S_{ij}^{\mathrm{f}}] + V_{\mathrm{m}}[S_{ij}^{\mathrm{m}}][A_{ij}])(V_{\mathrm{f}}[I] + V_{\mathrm{m}}[A_{ij}])^{-1}. \tag{5}$$

$[S_{ij}^{\mathrm{f}}]$ and $[S_{ij}^{\mathrm{m}}]$ are the compliance tensors of fiber and matrix, respectively. One can solve the bridging tensor from *Eq.* 5. We adopt Bridging Model [22] to calculate internal stresses for its simple explicit expression and better accuracy compared with some other famous models [23–25].

With Bridging Model [22], the stresses in fibers and matrix of a UD composite subjected to an arbitrary load $\{\sigma_{11}^0,\sigma_{22}^0,\sigma_{33}^0,\sigma_{23}^0,\sigma_{13}^0,\sigma_{12}^0\}$ can be easily obtained:

$$\sigma_{11}^{\mathrm{f}}=\frac{\sigma_{11}^0}{V_{\mathrm{f}}+V_{\mathrm{m}}A_{11}}-\frac{V_{\mathrm{m}}a_{12}(\sigma_{22}^0+\sigma_{33}^0)}{(V_{\mathrm{f}}+V_{\mathrm{m}}A_{11})(V_{\mathrm{f}}+V_{\mathrm{m}}A_{22})},\tag{6.1}$$

$$\sigma_{11}^{\mathrm{m}}=\frac{A_{11}\sigma_{11}^0}{V_{\mathrm{f}}+V_{\mathrm{m}}A_{11}}+\frac{V_{\mathrm{f}}A_{12}(\sigma_{22}^0+\sigma_{33}^0)}{(V_{\mathrm{f}}+V_{\mathrm{m}}A_{11})(V_{\mathrm{f}}+V_{\mathrm{m}}A_{22})},\tag{6.2}$$

$$\sigma_{22}^{\mathrm{f}}=\frac{\sigma_{22}^0}{V_{\mathrm{f}}+V_{\mathrm{m}}A_{22}},\ \sigma_{22}^{\mathrm{m}}=\frac{A_{22}\sigma_{22}^0}{V_{\mathrm{f}}+V_{\mathrm{m}}A_{22}},\tag{6.3,6.4}$$

$$\sigma_{23}^{\mathrm{m}}=\frac{A_{22}\sigma_{23}^0}{V_{\mathrm{f}}+V_{\mathrm{m}}A_{22}},\ \sigma_{12}^{\mathrm{m}}=\frac{A_{66}\sigma_{12}^0}{V_{\mathrm{f}}+V_{\mathrm{m}}A_{66}},\tag{6.5,6.6}$$

$$A_{11}=E^{\mathrm{m}}/E_{11}^{\mathrm{f}},A_{22}=A_{33}=A_{44}=0.3+0.7\frac{E^{\mathrm{m}}}{E_{22}^{\mathrm{f}}},\tag{7.1,7.2}$$

$$A_{55}=A_{66}=0.3+0.7\frac{G^{\mathrm{m}}}{G_{12}^{\mathrm{f}}},A_{12}=A_{13}=\frac{E_{11}^{\mathrm{f}}\nu^{\mathrm{m}}-E^{\mathrm{m}}\nu_{12}^{\mathrm{f}}}{E_{11}^{\mathrm{f}}-E^{\mathrm{m}}}(A_{22}-A_{11}).\tag{7.3,7.4}$$

Other A_{ij}'s are all zero. E_{11}^{f}, E_{22}^{f}, G_{12}^{f}, and ν_{12}^{f} are longitudinal, transverse, in-plane shear moduli, and longitudinal Poisson's ratio of fiber, respectively. E^{m} and ν^{m} are Young's modulus and Poisson's ratio of matrix, respectively, which have a relationship with in-plane shear moduli as $G^{\mathrm{m}} = 0.5E^{\mathrm{m}}/(1 + \nu^{\mathrm{m}})$.

MAIN BARRIER TO STRENGTH PREDICTION

Based on a micromechanical model, what prediction accuracy can be reached for the strength of composites? Let us consider, for example, the E-Glass/LY556 UD composite used in World-Wide Failure Exercise [26] and attempt to calculate its transverse tensile strength, σ_{22}^0. According to the component materials' properties provided by Ref. [26], the homogenized internal stresses are calculated from *Eqs.* 6.1-6.4:

$$\sigma_{11}^{\mathrm{f}}=-0.082\sigma_{22}^0,\sigma_{22}^{\mathrm{f}}=1.342\sigma_{22}^0,\sigma_{11}^{\mathrm{m}}=0.134\sigma_{22}^0,\sigma_{22}^{\mathrm{m}}=0.442\sigma_{22}^0.\tag{8}$$

Hence, the transverse tensile failure of the composite occurs when

$$\sigma_{22}^{\mathrm{u,t}}=\min\{Y_{\mathrm{f}}/1.342,\ \ Y_{\mathrm{m}}/0.442\},\tag{9}$$

where Y_{f} and Y_{m} are the transverse tensile strengths of fibers and matrix, respectively. For a composite subjected to transverse tensile load, the matrix tends to be destroyed first, thus one has $\sigma_{22}^{\mathrm{u,t}}=Y_{\mathrm{m}}/0.422$ here. The most straightforward way to determine Y_{m} is making it equal to the original tensile strength of matrix, hence one has $Y_{\mathrm{m}}=\sigma_{\mathrm{u,t}}^{\mathrm{m}}=80\,\mathrm{MPa}$ for LY556 epoxy [26]. If so, however, the predicted transverse tensile strength will be $\sigma_{22}^{\mathrm{u,t}}=181\,\mathrm{MPa}$, which is ~5.2 times as the corresponding measurement, 35 MPa [26].

This example is not a special case of strength prediction based on micromechanics, indicating a significant error due to direct application of original components' information and homogenized stresses. There are two ways to overcome this barrier. One is replacing original strengths of component materials with corresponding real allowable strengths. The other is converting homogenized internal stresses calculated from *Eqs.* 3 and 4 into "true" values. We choose the second way because it is more applicable to step-by-step loading conditions. The point-wise stresses in a fiber are uniform [27,28], thus its homogenized and true stresses are the same. However, stresses in matrix are not uniform. Applying uniaxial tensile load to a plate with a hole on it leads to stress concentration. Similarly, if the hole is filled with a fiber, stress concentration generates as well. Therefore, each of the true stress components is obtained by multiplying the homogenized internal stress with a corresponding factor, which is called stress concentration factor (SCF) [20,21].

TRANSVERSE SCFS WITH PERFECT INTERFACIAL BONDING

However, such an SCF cannot be defined in the classical way by dividing the maximum point stress by the surface-averaged stress. Instead, the new definition here is the ratio of a line-averaged stress and the corresponding volume-averaged stress of matrix. The SCFs of a composite subjected to transverse tension, transverse compression, and transverse shear, respectively, have already been derived in previous work [20,21]. For completeness, they are briefly introduced below.

The SCF of the matrix subjected to a transverse load is derived through [21]

$$K_{22}(\varphi)=\frac{1}{|\vec{\mathrm{R}}_{\varphi}^{b}-\vec{\mathrm{R}}_{\varphi}^{a}|}\int_{|\vec{R}_{\varphi}^{a}|}^{|\vec{R}_{\varphi}^{b}|}\frac{\tilde{\sigma}_{22}^{\mathrm{m}}}{(\sigma_{22}^{\mathrm{m}})_{\mathrm{BM}}}d|\vec{R}_{\varphi}|.\tag{10}$$

Symbols in *Eq.* 10 are introduced with illustrative Fig. 1, which shows a representative volume element (RVE) of a composite subjected to uniaxial load σ_{22}^0. $\tilde{\sigma}_{22}^{\mathrm{m}}$ is the stress distribution of matrix along the loading direction calculated with CCA model (concentric cylinder assemblage). $(\sigma_{22}^{\mathrm{m}})_{\mathrm{BM}}$ is the corresponding homogenized stress obtained from *Eq.* 6.4. The integral direction angle φ is defined as the inclined angle between the loading direction and the outward normal vector of failure surface. $\vec{R}_{\varphi}^{\mathrm{a}}$ and $\vec{R}_{\varphi}^{\mathrm{b}}$ are vectors along the integral direction, both starting from origin, but ending at the surfaces of fiber and

DOI 10.1002/pc

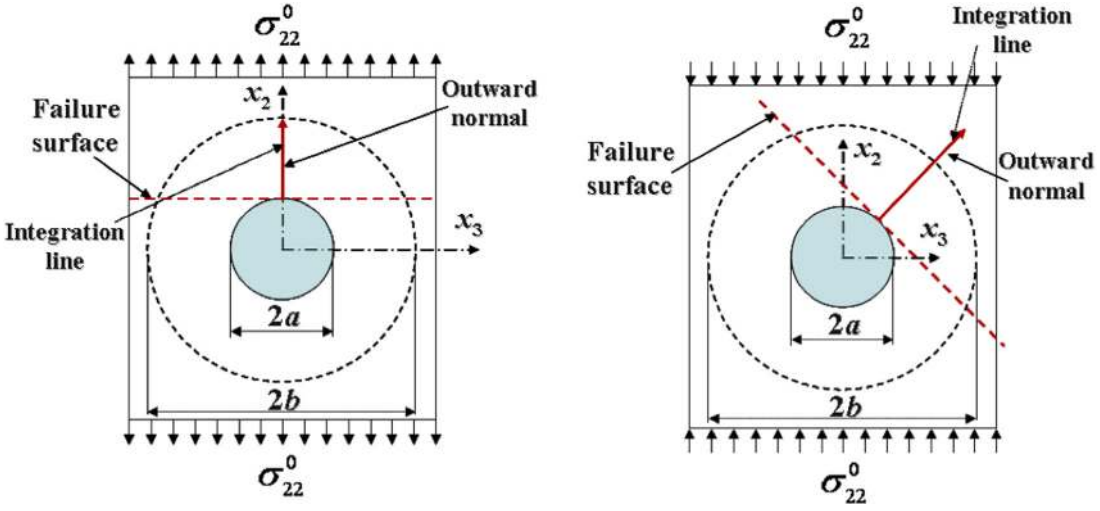

FIG. 1. Schematic of a RVE used in defining SCF of matrix in a composite subjected to (a) a transverse tension (b) a transverse compression.

matrix cylinders, respectively (Fig. 1), with superscript a and b representing their lengths, which can be related by V_f as

$$b = a/\sqrt{V_f}. \tag{11}$$

Explicit expression of *Eq.* 10 is [21]

$$K_{22}(\varphi) = \left\{1 + \frac{A}{2}\sqrt{V_f}\cos 2\varphi + \frac{B}{2(1-\sqrt{V_f})}[V_f^2\cos 4\varphi + 4V_f(\cos\varphi)^2 (1-2\cos 2\varphi) + \sqrt{V_f}(2\cos 2\varphi + \cos 4\varphi)]\right\}(V_f + A_{22}V_m)/A_{22}, \tag{12.1}$$

$$A = \frac{2E_{22}^f E^m (\nu_{12}^f)^2 + E_{11}^f\{E^m(\nu_{23}^f - 1) - E_{22}^f[2(\nu^m)^2 + \nu^m - 1]\}}{E_{11}^f[E_{22}^f + E^m(1-\nu_{23}^f) + E_{22}^f\nu^m] - 2E_{22}^f E^m(\nu_{12}^f)^2}, \tag{12.2}$$

$$B = \frac{E^m(1+\nu_{23}^f) - E_{22}^f(1+\nu^m)}{E_{22}^f[\nu^m + 4(\nu^m)^2 - 3] - E^m(1+\nu_{23}^f)}, \tag{12.3}$$

where ν_{23}^f is the transverse Poisson's ratio of fiber. For a composite under uniaxial transverse tension, the fracture surface is perpendicular to the loading direction, thus the parameter φ in *Eq.* 10 equals to 0 (Fig. 1a). However, for a composite under uniaxial transverse compression, φ equals to an acute angle ϕ (Fig. 1b), which can be determined with Mohr's theory [21]:

$$\phi = \frac{\pi}{4} + \frac{1}{2}\arcsin\frac{\sigma_{u,c}^m - \sigma_{u,t}^m}{2\sigma_{u,c}^m} \tag{13}$$

Hence, the transverse tensile and compressive SCFs are calculated from *Eq.* 12 as $K_{22}^t = K_{22}(0)$ and $K_{22}^c = K_{22}(\phi)$ respectively. The transverse shear SCF of matrix is obtained with Mohr's theory [21]:

$$K_{23} = 2\sigma_{u,s}^m\sqrt{\frac{K_{22}^t K_{22}^c}{\sigma_{u,t}^m\sigma_{u,c}^m}}. \tag{14}$$

$\sigma_{u,t}^m$, $\sigma_{u,c}^m$, and $\sigma_{u,s}^m$ are original tensile, compressive, and shear strengths of matrix, respectively.

OTHER SCFSs WITH PERFECT INTERFACIAL BONDING

SCF Under Longitudinal Shear

Equation 10 stands for the general way to derive a SCF of matrix. It is clear that the key point to definite an SCF is determining the integral line according to the fracture surface orientation and the stress component on the numerator of *Eq.* 10. Under a longitudinal shear load, the failure surface of a UD composite is shown in Fig. 2 [29,30]. Following *Eq.* 10, the longitudinal shear SCF is given by (Fig. 3)

$$K_{12}(\varphi) = \frac{1}{\sqrt{2}[\sqrt{b^2 - (a\sin\varphi)^2} - a\cos\varphi]} \int_0^{\sqrt{2}[\sqrt{b^2-(a\sin\varphi)^2}-a\cos\varphi]} \frac{\tilde{\sigma}_{12}^m}{(\sigma_{12}^m)_{BM}} dS.$$

$\tilde{\sigma}_{12}^m$ is the in-plane shear stress of matrix, obtained from CCA model as [28]

$$\tilde{\sigma}_{12}^m = \sigma_{12}^0\left[1 - a^2\frac{(G_{12}^f - G^m)(x_2^2 - x_3^2)}{(G_{12}^f + G^m)(x_2^2 + x_3^2)^2}\right]. \tag{16}$$

$(\sigma_{12}^m)_{BM}$ is calculated from *Eq.* 6.6. Substituting *Eqs.* 16 and 6.6 into *Eq.* 15 leads to

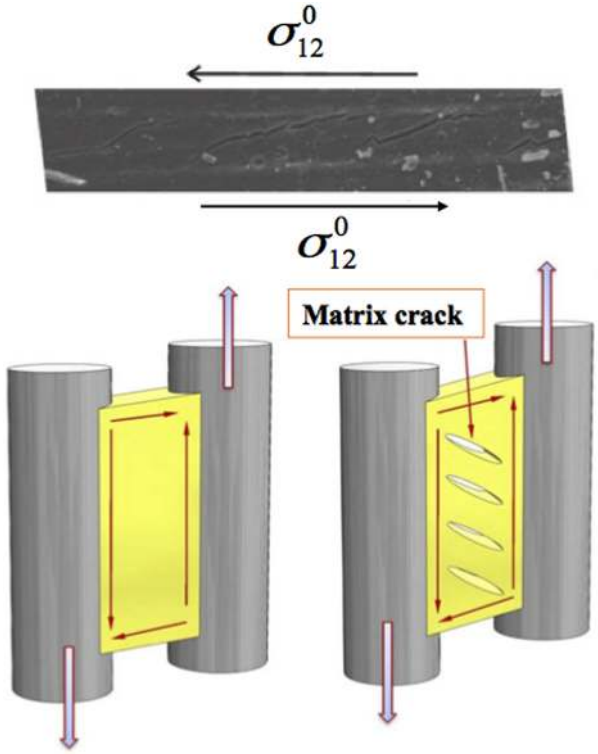

FIG. 2. Failures of the matrix in a composite under a longitudinal shear.

$$K_{12}(\varphi)=\left[1-\frac{(G_{12}^{f}-G^{m})\{\sqrt{V_f}\cos\varphi-V_f\sqrt{1-V_f(\sin\varphi)^2}\}}{(G_{12}^{f}+G^{m})\{\sqrt{(1-V_f(\sin\varphi)^2)}-\sqrt{V_f}\cos\varphi\}}\right]\frac{(V_f+A_{66}V_m)}{A_{66}}. \tag{17}$$

Under a transverse load, the matrix transverse stress component in CCA model is uniform along the direction parallel to fiber (along the x_1-axial) [28]. However, a longitudinal shear load results in nonuniform shear stress distribution along the thickness direction (along the x_3-axial), as seen from *Eq.* 16 and Fig. 3. Thus, it is necessary to average the results of *Eq.* 17 along the thickness direction, that is

$$\begin{aligned}K_{12}&=\frac{1}{2a}\int_{-a}^{a}K_{12}(x_3)(dx_3)=\frac{1}{\pi a}\int_{-\pi/2}^{\pi/2}K_{12}(\varphi)\cos(\varphi)(ad\varphi)\\&=\left[1-V_f\frac{G_{12}^{f}-G^{m}}{G_{12}^{f}+G^{m}}\left\{W(V_f)-\frac{1}{3}\right\}\right]\frac{(V_f+A_{66}V_m)}{A_{66}},\end{aligned} \tag{18.1}$$

$$W(V_f)=\int_0^a\frac{1}{a}\sqrt{1-\frac{x_3^2}{a^2}}\sqrt{\frac{1}{V_f}-\frac{x_3^2}{a^2}}dx_3$$

$$\approx\pi\sqrt{V_f}\left[\frac{1}{4V_f}-\frac{4}{128}-\frac{2}{512}V_f-\frac{5}{4096}V_f^2\right].$$

Longitudinal Normal SCF

For a CCA model subjected to longitudinal tension or compression, the stresses in matrix are uniform [28], thus no stress concentration occurs. Therefore, the longitudinal normal SCF of composites equals to one.

SCF WITH INTERFACIAL CRACKS

In our previous work, all SCFs are derived based on an assumption of a perfect fiber/matrix interfacial bonding. However, interfacial cracks were actually widely observed in composites under various loading conditions [18,31,32]. Considering the significant effects of interfacial debonding on ultimate strengths, it is necessary to derive the SCF for the composites after interfacial cracks.

Supposing that there is a stable crack with central angle of 2Ψ on the fiber/matrix interface of a CCA model subjected to uniaxial tension, as shown in Fig. 4, the stress field of matrix was derived by Toya [33] with the stress

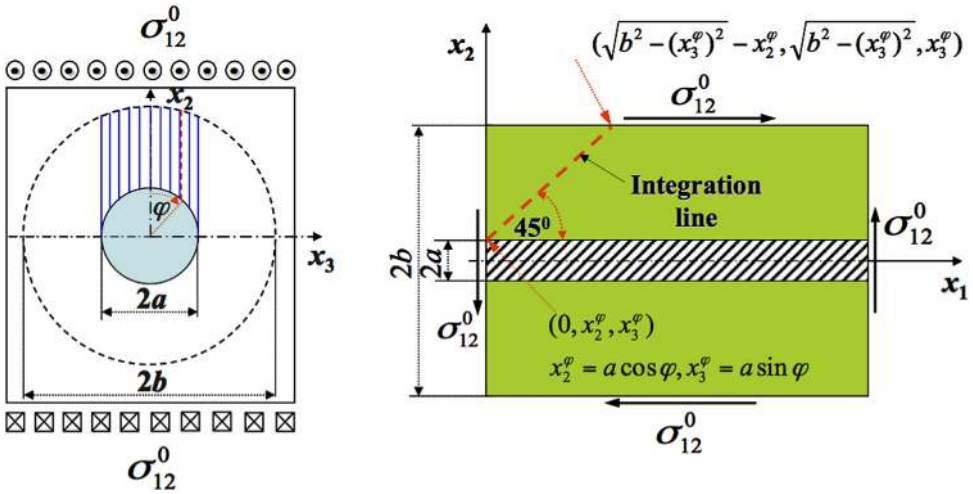

FIG. 3. Schematic definition for the SCF of matrix under a longitudinal shear.

 DOI 10.1002/pc

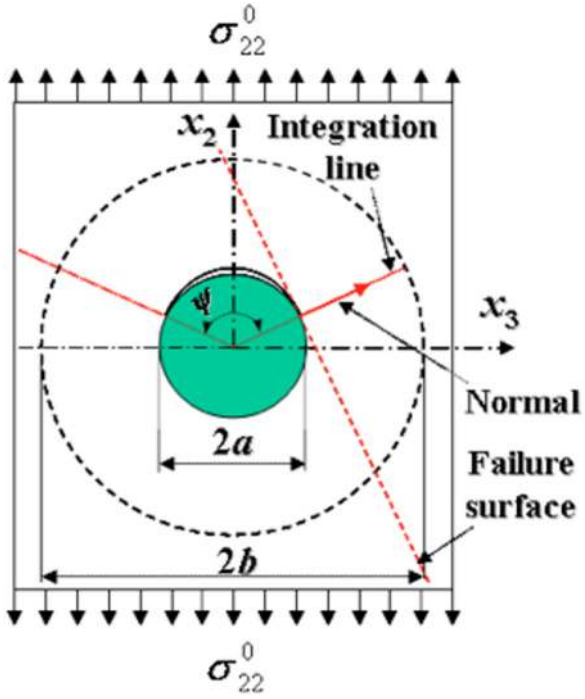

FIG. 4. Schematic failure of a transverse tensile-loaded composite with an interface crack.

component along the loading direction given by (Appendix A):

$$\tilde{\sigma}_{22}^{\mathrm{m}}=\frac{\sigma_{22}^0}{2}\mathrm{Re}\left[2M(z)+\left(\frac{a^2}{z}-\bar{z}\right)M'(z)-\frac{a^2}{z^2}\left\{\overline{M}\left(\frac{a^2}{z}\right)+M(z)\right\}\right], \tag{19.1}$$

$$M(z)=F-\frac{a^2k}{z^2}-\left[(F-0.5)z+H+\frac{C}{z}+\frac{D}{z^2}\right]\chi(z)=\overline{M}(z), \tag{19.2}$$

$$F=\frac{1-(\cos\psi+2\lambda\sin\psi)\exp[2\lambda(\pi-\psi)]+(1-k)(1+4\lambda^2)\sin^2\psi}{\frac{4}{k}-2-2(\cos\psi+2\lambda\sin\psi)\exp[2\lambda(\pi-\psi)]}, \tag{19.3}$$

$$H=a(\cos\psi+2\lambda\sin\psi)(0.5-F), \tag{19.4}$$

$$C=(k-1)(\cos\psi-2\lambda\sin\psi)a^2\exp[2\lambda(\psi-\pi)], \tag{19.5}$$

$$D=(1-k)a^3\exp[2\lambda(\psi-\pi)], \tag{19.6}$$

$$\chi(z)=(z-ae^{i\psi})^{-0.5+i\lambda}(z-ae^{-i\psi})^{-0.5-i\lambda}, \tag{19.7}$$

$$k=\frac{\mu_1(1+\kappa_2)}{(1+\xi)(\mu_1+\kappa_1\mu_2)},\lambda=-(ln\xi)/(2\pi),\xi=(\mu_2+\kappa_2\mu_1)/(\mu_1+\kappa_1\mu_2). \tag{19.8}$$

$$\kappa_1=\frac{3-\nu^{\mathrm{m}}}{1+\nu^{\mathrm{m}}},\kappa_2=\frac{3-\nu^{\mathrm{f}}}{1+\nu^{\mathrm{f}}},\mu_1=\frac{E^{\mathrm{m}}(\kappa_1-1)\nu^{\mathrm{m}}}{\left[1-(\nu_{\mathrm{m}})^2\right](3-\kappa_1)},\mu_2=\frac{E^{\mathrm{f}}(\kappa_2-1)\nu^{\mathrm{f}}}{\left[1-(\nu^{\mathrm{f}})^2\right](3-\kappa_2)}, \tag{19.9}$$

The solution above is only applicable to plane stress problems with isotropic fibers and matrix. To extend the application scope of this method to plane strain cases, according to the well-known relationship between plane stress and plane strain states, only the elastic modulus and Poisson's ratio need to be replaced by

$$E=\frac{E_{22}}{1-\nu_{12}\nu_{21}}\text{ and }\nu=\frac{\nu_{23}+\nu_{12}\nu_{21}}{1-\nu_{12}\nu_{21}}.$$

Accordingly, *Eq.* 19.9 is changed into

$$\kappa_1=3-4\nu^{\mathrm{m}},\kappa_2=\frac{3-\nu_{23}^{\mathrm{f}}-4\nu_{12}^{\mathrm{f}}\nu_{21}^{\mathrm{f}}}{1+\nu_{23}^{\mathrm{f}}},\mu_1=\frac{E^{\mathrm{m}}}{2(1+\nu^{\mathrm{m}})},\mu_2=\frac{E_{22}^{\mathrm{f}}}{2(1+\nu_{23}^{\mathrm{f}})}. \tag{20}$$

Substituting *Eqs.* 19, 11, 6.4, *and* 20 into *Eq.* 10 results in (Appendix B)

$$\hat{K}_{22}^t(\varphi)=\mathrm{Re}\left\{e^{-2i\varphi}M(b')(a^2/b-b)+e^{-i\varphi}\left(N_1\left(\frac{a^2}{b'}\right)-N_1\left(\frac{a^2}{a'}\right)\right)+e^{-i\varphi}(2+e^{-2i\varphi})[N(b')-N(a')]\right\}\frac{(V_{\mathrm{f}}+0.3V_{\mathrm{m}})E_{22}^{\mathrm{f}}+0.7V_{\mathrm{m}}E^{\mathrm{m}}}{2(b-a)(0.3E_{22}^{\mathrm{f}}+0.7E^{\mathrm{m}})}, \tag{21.1}$$

$$N(z)=Fz+\frac{a^2k}{z}-(z-ae^{i\psi})^{0.5+i\lambda}(z-ae^{-i\psi})^{0.5-i\lambda}\left[(F-0.5)-\frac{D}{a^2z}\right], \tag{21.2}$$

$$N_1(z)=Fz+\frac{a^2k}{z}+\frac{1}{\xi}(z-ae^{i\psi})^{0.5+i\lambda}(z-ae^{-i\psi})^{0.5-i\lambda}\left[(F-0.5)-\frac{D}{a^2z}\right], \tag{21.3}$$

where $a'=a(\cos\varphi+i\sin\varphi)$ and $b'=b(\cos\varphi+i\sin\varphi)$. We use "^" on head to represent quantities relevant to the condition of interfacial debonding.

To calculate the transverse tensile SCF of a composite with interfacial cracks, which is denoted as$\hat{K}_{22}^t$, the integral direction angle φ must be reconsidered. As the transverse cross section of a UD composite is isotropic, it is likely that a tensile load applied in this plane would result in fracture occurring along the direction of the maximum line-averaged stress. In other words, $\hat{K}_{22}^t$ equals to the maximum value of $\hat{K}_{22}^t(\varphi)$, given by

$$\begin{aligned}\hat{K}_{22}^t&=\hat{K}_{22}^t(\psi)=\max\left\{\hat{K}_{22}^t(\varphi),0^\circ\le\varphi\le90^\circ\right\}\\&=\mathrm{Re}\left\{e^{-2i\psi}M(be^{i\psi})(a^2/b-b)-e^{-i\psi}\left(N_2-N_1\left(\frac{a^2}{b}e^{-i\psi}\right)\right)+e^{-i\psi}(2+e^{-2i\psi})[N(be^{i\psi})-N_3]\right\}\frac{(V_{\mathrm{f}}+0.3V_{\mathrm{m}})E_{22}^{\mathrm{f}}+0.7V_{\mathrm{m}}E^{\mathrm{m}}}{2(b-a)(0.3E_{22}^{\mathrm{f}}+0.7E^{\mathrm{m}})},\end{aligned} \tag{22.1}$$

$$N_2=aFe^{-i\psi}+ake^{i\psi},N_3=Fae^{i\psi}+e^{-i\psi}ak. \tag{22.2}$$

Hobbiebrunken et al. have shown in the fig. 7 of Ref. [18] that the fracture surface of a composite after interfacial debonding tends to initiate from interfacial crack tips [18], which is consistent with the starting point of our integral line.

At last, let us discuss how to determine the center angle of interfacial cracks, which is denoted by 2Ψ. Owing to Poisson's deformation, a part of fiber/matrix interface near to the coordinate axis perpendicular to applied load (x_3-axial in **Fig**. 4) will be in the compressive state. Thus, there must be a terminal point for interfacial crack propagation. At this terminal point, the interfacial crack will not continue to expand, for which the critical condition is that the radial relative displacement between fiber and matrix faces at the crack tip equals to 0. Based on Toya's solution [33], this critical condition is written as (Appendix C)

$$\mathrm{Re}\left\{\left(G_0-\frac{1}{k}-\frac{2(1-k)}{k\exp(i\varphi)}\exp[2\lambda(\psi-\pi)]\right)R\left(e^{i\varphi}\right)\right\}_{\varphi=\psi-\gamma}=0, \tag{23}$$

$$G_0=\frac{1-(\cos\psi+2\lambda\sin\psi)\exp[2\lambda(\pi-\psi)]+(1-k)(1+4\lambda^2)\sin^2\psi}{2-k-k(\cos\psi+2\lambda\sin\psi)\exp[2\lambda(\pi-\psi)]}, \tag{24.1}$$

$$R(\exp(i\varphi))=\left[\exp(i(\varphi))-e^{i\psi}\right]^{0.5+i\lambda}\left[\exp(i(\varphi))-e^{-i\psi}\right]^{0.5-i\lambda}\exp(-i(\varphi)), \tag{24.2}$$

$$\gamma=\frac{2\lambda(J_1^2+J_2^2)}{J_1^2+J_2^2-2J_2J_3},\text{if}\,\xi<1, \tag{25.1}$$

$$\gamma=-\frac{2\lambda(J_1^2+J_2^2)}{J_1^2+J_2^2-2J_2J_3},\text{if}\,\xi>1, \tag{25.2}$$

$$J_1=kG_0-1-2(1-k)\xi\exp(2\lambda\psi)\cos(\psi), \tag{25.3}$$

$$J_2=2(1-k)\xi\exp(2\lambda\psi)\sin(\psi), \tag{25.4}$$

$$J_3=2(1-k)\xi\exp(2\lambda\psi)[J_1\cos(\psi)-J_2\sin(\psi)]/J_2. \tag{25.5}$$

Substituting γ obtained from *Eqs.* 25.1 *or* 25.2 *into Eq.* 23, the debonding angle 2Ψ can be solved, with the SCF $\hat{K}_{22}^t$ determined from *Eq.* 22.

It is noted that if $\gamma = 0$, a singular solution of Ψ will be obtained from *Eq.* 23. There always exist deviations in the measurements of original fiber and matrix properties. Therefore, for this special case, it is acceptable to adjust slightly a certain fiber or matrix mechanical property parameter to avoid the singular solution.

INTERFACIAL CRACK DETECTION

In general, the fiber/matrix interface of a composite is initially bonded perfectly before being applied any load. Considering a UD composite subjected to uniaxial transverse tensile loadσ_{22}^0, when the applied stress is increased to a certain level, for example, $\hat{\sigma}_{22}^0$, interfacial debonding happens. Many reports have pointed out that, once debonding occurs the interfacial cracks tend to develop rapidly into the final stable state [18,34,35]. Therefore, it is reasonable to neglect the brief process of this unstable interfacial crack propagation, during which the debonding angle 2φ grows from 0 to 2Ψ and the applied load only increases slightly. For simplicity, the whole loading process is divided into two stages, between which the point of demarcation is the load level when interfacial cracks appear. The central angles of interfacial cracks in these two stages are 0 and 2Ψ, respectively, with the corresponding SCFs beingK_{22}^t and$\hat{K}_{22}^t$.

From *Eq.* 6.4, the transverse stress component in matrix when debonding occurs is

$$\hat{\sigma}_{22}^{\mathrm{m}}=\frac{0.3E_{22}^{\mathrm{f}}+0.7E^{\mathrm{m}}}{(V_{\mathrm{f}}+0.3V_{\mathrm{m}})E_{22}^{\mathrm{f}}+0.7V_{\mathrm{m}}E^{\mathrm{m}}}\hat{\sigma}_{22}^0. \tag{26.1}$$

Furthermore, the corresponding longitudinal stress is obtained from *Eq.* 6.2:

$$\hat{\sigma}_{11}^{\mathrm{m}}=\frac{V_{\mathrm{f}}A_{12}}{(V_{\mathrm{f}}+V_{\mathrm{m}}A_{11})(V_{\mathrm{f}}+V_{\mathrm{m}}A_{22})}\hat{\sigma}_{22}^0. \tag{26.2}$$

Supposing that the transverse stress in the matrix when final failure occurs is $\sigma_{22}^{\mathrm{m},Y}$ and the composite's ultimate transverse tensile strength is Y, one gets

$$\hat{K}_{22}^t(\sigma_{22}^{\mathrm{m},Y}-\hat{\sigma}_{22}^{\mathrm{m}})+K_{22}^t\hat{\sigma}_{22}^{\mathrm{m}}=\sigma_{\mathrm{u,t}}^{\mathrm{m}}, \tag{27.1}$$

where

$$\sigma_{22}^{\mathrm{m},Y}-\hat{\sigma}_{22}^{\mathrm{m}}=\frac{0.3E_{22}^{\mathrm{f}}+0.7E^{\mathrm{m}}}{(V_{\mathrm{f}}+0.3V_{\mathrm{m}})E_{22}^{\mathrm{f}}+0.7V_{\mathrm{m}}E^{\mathrm{m}}}\left(Y-\hat{\sigma}_{22}^0\right). \tag{27.2}$$

From *Eqs.* 26.1, 27.1, *and* 27.2, the critical transverse tensile load is derived:

$$\hat{\sigma}_{22}^0=\frac{\hat{K}_{22}^tY}{\hat{K}_{22}^t-K_{22}^t}-\frac{(V_{\mathrm{f}}+0.3V_{\mathrm{m}})E_{22}^{\mathrm{f}}+0.7V_{\mathrm{m}}E^{\mathrm{m}}}{(0.3E_{22}^{\mathrm{f}}+0.7E^{\mathrm{m}})(\hat{K}_{22}^t-K_{22}^t)}\sigma_{\mathrm{u,t}}^{\mathrm{m}}. \tag{28}$$

If the value of *Eq.* 28 of a composite is near to, equal to, or greater than the transverse tensile strength, the material can be considered to have a sufficiently strong interface that can bring component materials' strengths into full play. Otherwise, the material system will undergo interfacial debonding, which significantly influences the load carrying capacity of the composite. It can be seen that the intuitive information given by *Eq.* 28 is valuable for jugging the necessity of interfacial modification.

The last question is which quantity should be chosen to judge whether interfacial debonding would occur in a given material system under a certain loading condition. It is likely that von Mises stress would be suitable because it can represent the comprehensive stress level well. A critical von Mises stress obtained from true stresses of matrix is defined as

$$\hat{\sigma}_e^{\mathrm{m}}=\sqrt{(\hat{\sigma}_{11}^{\mathrm{m}})^2+\left(K_{22}^t\hat{\sigma}_{22}^{\mathrm{m}}\right)^2-K_{22}^t\hat{\sigma}_{11}^{\mathrm{m}}\hat{\sigma}_{22}^{\mathrm{m}}}. \tag{29}$$

When the composite is subjected to a planar step-by-step load, the von Mises stress of matrix at a certain loading step is determined through

 DOI 10.1002/pc

$$(\overline{\sigma}_e^{\mathrm{m}})_l=\sqrt{(\overline{\sigma}_{11}^{\mathrm{m}})_l^2+(\overline{\sigma}_{22}^{\mathrm{m}})_l^2-(\overline{\sigma}_{11}^{\mathrm{m}})_l(\overline{\sigma}_{22}^{\mathrm{m}})_l+3(\overline{\sigma}_{12}^{\mathrm{m}})_l^2}, \quad (30)$$

$$(\overline{\sigma}_{11}^{\mathrm{m}})_l=(\overline{\sigma}_{11}^{\mathrm{m}})_{l-1}+d\sigma_{11}^{\mathrm{m}}, \quad (31.1)$$

$$(\overline{\sigma}_{22}^{\mathrm{m}})_l=(\overline{\sigma}_{22}^{\mathrm{m}})_{l-1}+K_{22}d\sigma_{22}^{\mathrm{m}}, \quad (31.2)$$

$$(\overline{\sigma}_{12}^{\mathrm{m}})_l=(\overline{\sigma}_{12}^{\mathrm{m}})_{l-1}+K_{12}d\sigma_{12}^{\mathrm{m}}, \quad (31.3)$$

$$K_{22}=\begin{cases}K_{22}^t, & \text{if } d\sigma_{22}^{\mathrm{m}}>0 \text{ and before interface crack}\\ \hat{K}_{22}^t, & \text{if } d\sigma_{22}^{\mathrm{m}}>0 \text{ and after interface crack}\\ K_{22}^c, & \text{if } d\sigma_{22}^{\mathrm{m}}<0\end{cases}. \quad (32)$$

l is the sequence number of the loading step and $\{d\sigma_{11}^{\mathrm{m}}, d\sigma_{22}^{\mathrm{m}}, d\sigma_{12}^{\mathrm{m}}\}$ are the homogenized stress increments of matrix caused by the l-th loading increment. Applying the Bridging Model [21], $\{d\sigma_{11}^{\mathrm{m}}, d\sigma_{22}^{\mathrm{m}}, d\sigma_{12}^{\mathrm{m}}\}$ are calculated from *Eqs.* 6.2, 6.4, *and* 6.6 by replacing $\{\sigma_{11}^0,\sigma_{22}^0,\sigma_{12}^0\}$ with $\{d\sigma_{11}^0,d\sigma_{22}^0,d\sigma_{12}^0\}$.

If the first principal stress of matrix is positive, debonding occurs when

$$(\overline{\sigma}_{\mathrm{m}}^1)_I>0 \text{ and } (\sigma_e^{\mathrm{m}})_I\geq\hat{\sigma}_e^{\mathrm{m}}, \quad (33)$$

where $(\overline{\sigma}_{\mathrm{m}}^1)_l$ is the first principal stress obtained from $\{(\overline{\sigma}_{11}^{\mathrm{m}})_l,(\overline{\sigma}_{22}^{\mathrm{m}})_l,(\overline{\sigma}_{33}^{\mathrm{m}})_l\}$. It can be seen from *Eqs.* 30 *and* 33 that interfacial debonding is caused by not only transverse tensile stress, but also other stress components. However, the effects of debonding on composite materials' strengths along other directions are less significant than that on the transverse tensile strength [18,34,35]. Therefore, in this work, only the transverse tensile strength of a composite is chosen as the input parameter to represent the quality of interface, while loads applied from other directions are also considered when judge whether interfacial debonding occurs.

The failure strength of a composite is determined by estimating the carrying capacities of the component materials respectively. Tsai-Wu's criterion is used to determine whether the matrix is destroyed under a given loading condition, while generalized maximum normal stress failure criterion [22] is applied to fiber. Thus the conditions of material failure can be written as

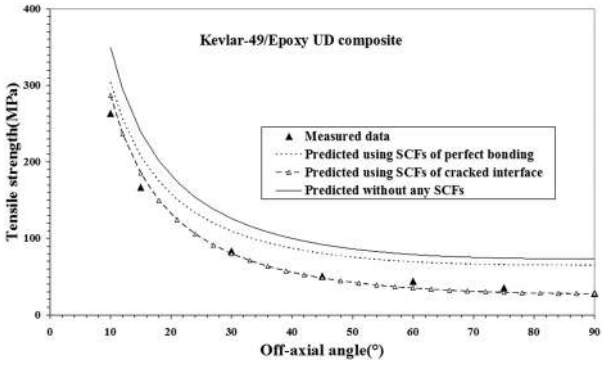

FIG. 5. Comparison of different schemes' predictions with experiments [41] for off-axial tensile strengths of a Kevlar-49/epoxy UD composite.

$$F_1\left[(\overline{\sigma}_{11}^{\mathrm{m}})_l^2+(\overline{\sigma}_{22}^{\mathrm{m}})_l^2-(\overline{\sigma}_{11}^{\mathrm{m}})_l(\overline{\sigma}_{22}^{\mathrm{m}})_l\right]+F_2(\overline{\sigma}_{12}^{\mathrm{m}})_l^2 +F_3\left[(\overline{\sigma}_{11}^{\mathrm{m}})_l+(\overline{\sigma}_{22}^{\mathrm{m}})_l\right]\geq 1, \quad (34.1)$$

$$F_1=1/(\sigma_{\mathrm{u,t}}^{\mathrm{m}}\sigma_{\mathrm{u,c}}^{\mathrm{m}}), F_2=1/(\sigma_{\mathrm{u,s}}^{\mathrm{m}})^2, F_3=1/\sigma_{\mathrm{u,t}}^{\mathrm{m}}-1/\sigma_{\mathrm{u,c}}^{\mathrm{m}}. \quad (34.2)$$

$$(\sigma_{\mathrm{eq,t}}^{\mathrm{f}})_l\geq\sigma_{\mathrm{u,t}}^{\mathrm{f}} \text{ or } (\sigma_{\mathrm{eq,c}}^{\mathrm{f}})_l\geq-\sigma_{\mathrm{u,c}}^{\mathrm{f}}, \quad (35.1)$$

$$(\sigma_{\mathrm{eq,t}}^{\mathrm{f}})_l=\begin{cases}(\sigma_{\mathrm{f}}^1)_l, & \text{if } (\sigma_{\mathrm{f}}^3)_l<0,\\ [(\sigma_{\mathrm{f}}^1)_l^3+(\sigma_{\mathrm{f}}^2)_l^3]^{\frac{1}{3}}, & \text{if } (\sigma_{\mathrm{f}}^3)_l=0\end{cases}, \quad (35.2)$$

$$(\sigma_{\mathrm{eq,c}}^{\mathrm{f}})_l=\begin{cases}(\sigma_{\mathrm{f}}^3)_l, & \text{if } (\sigma_{\mathrm{f}}^1)_l>0,\\ (\sigma_{\mathrm{f}}^3)_l-(\sigma_{\mathrm{f}}^1)_l & \text{if } (\sigma_{\mathrm{f}}^1)_l\leq 0\end{cases}. \quad (35.3)$$

where $(\sigma_{\mathrm{f}}^1)_l$, $(\sigma_{\mathrm{f}}^2)_l$, and $(\sigma_{\mathrm{f}}^3)_l$ are the three principal stresses of the fiber.

ILLUSTRATION

For validating the method proposed in this article, Kevlar-49 fiber/epoxy and E-glass fiber/8804 epoxy UD composites are chosen as examples, with their components' properties and transverse strengths listed as known conditions. Besides, with the constituent thermoelastic properties, the thermal residual stresses are calculated by applying the micromechanical method in Ref. [36] and considered together with applied stress in final failure analysis. To illustrate how to utilize the method put forward in this article, the procedure for calculating the off-axial tensile strengths of the two composites will be introduced step by step, with the predicted results compared with corresponding measurements.

With the components' information of two composites gained from Refs. [37–40], the corresponding SCFs are calculated for later usage. The original parameters of Kevlar-49 fiber/epoxy materials used in Fig. 5 are [37,38] $E_{11}^{\mathrm{f}}=124.1$ GPa, $E_{22}^{\mathrm{f}}=4.1$ GPa, $E_{22}^{\mathrm{f}}=4.1$ GPa, $\nu_{12}^{\mathrm{f}}=\nu_{23}^{\mathrm{f}}=0.35$, $\sigma_{\mathrm{u,t}}^{\mathrm{f}}=2060$ MPa, $\alpha_{11}^{\mathrm{f}}=-5.7\sigma_{\mathrm{u,t}}^{\mathrm{f}}=2060.\times10^{-6^\circ}\mathrm{C}^{-1}$, $\alpha_{22}^{\mathrm{f}}=\alpha_{33}^{\mathrm{f}}\times10^{-6^\circ}\mathrm{C}^{-1}$, $E^{\mathrm{m}}=3.45$ GPa, $\nu^{\mathrm{m}}=0.35$, $\sigma_{\mathrm{u,t}}^{\mathrm{m}}=69$ MPa, $\sigma_{\mathrm{u,c}}^{\mathrm{m}}=120$ MPa, $\sigma_{\mathrm{u,s}}^{\mathrm{m}}=50$ MPa, $\alpha^{\mathrm{m}}=65\times10^{-6^\circ}\mathrm{C}^{-1}$, and $V_{\mathrm{f}}=0.55$, while parameters calculated are $K_{22}^{\mathrm{t}}=1.08$, $K_{22}^{\mathrm{c}}=1.07$, $\hat{K}_{22}^{\mathrm{t}}=2.74$, and $K_{12}=1.17$. Correspondingly, the parameters of E-glass fiber/8804 epoxy materials used in Fig. 6 are [39,40]: $E_{11}^{\mathrm{f}}=71$ GPa, $G_{12}^{\mathrm{f}}=28.2$ GPa, $G_{12}^{\mathrm{f}}=28.2$ GPa, $\nu_{12}^{\mathrm{f}}=\nu_{23}^{\mathrm{f}}=0.26$, $\sigma_{\mathrm{u,t}}^{\mathrm{f}}=1500$ MPa, $\alpha_{11}^{\mathrm{f}}=6.9\times10^{-6^\circ}\mathrm{C}^{-1}$, $\alpha_{22}^{\mathrm{f}}=\alpha_{33}^{\mathrm{f}}=6.9\times10^{-6^\circ}\mathrm{C}^{-1}$, $E^{\mathrm{m}}=3.1$ GPa, $\nu^{\mathrm{m}}=0.29$, $\sigma_{\mathrm{u,t}}^{\mathrm{m}}=70$ MPa, $\sigma_{\mathrm{u,c}}^{\mathrm{m}}=86$ MPa, $\sigma_{\mathrm{u,s}}^{\mathrm{m}}=39$ MPa, $\alpha^{\mathrm{m}}=70\times10^{-6^\circ}\mathrm{C}^{-1}$ and $V_{\mathrm{f}}=0.51$, while SFCs are $K_{22}^{\mathrm{t}}=2.97$, $K_{22}^{\mathrm{c}}=2.02$, $\hat{K}_{22}^{\mathrm{t}}=5.61$ and $K_{12}=1.38$. The transverse tensile SCF of the Kevlar fiber reinforced system without interfacial cracks is close to 1, because the transverse modulus of the Kevlar fiber is close to that of the matrix. Nevertheless, the transverse tensile SCF of the Kevlar fiber reinforced system increases significantly after interfacial debonding. This change is even more obvious in

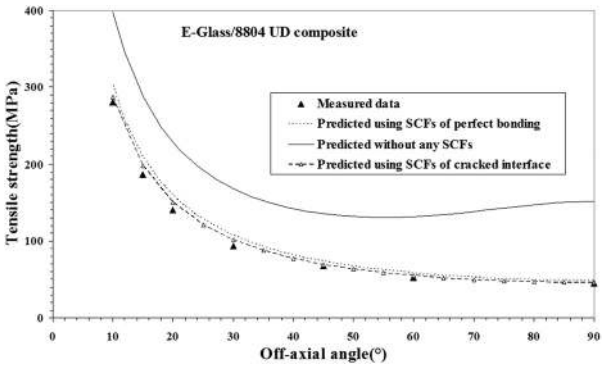

FIG. 6. Comparison of different schemes' predictions with experiments [39] for off-axial tensile strengths of a E-glass/8804 UD composite.

the E-glass fiber/8804 reinforced system. After investigating some other material systems used in World-Wide Failure Exercise [26], it was found that, on one hand, an increase in stress fluctuation intensity of matrix due to interfacial debonding is universal among various material composites. On the other hand, the stress fluctuation intensity, which is characterized by SCFs, plays an important role in determining the failure strength of composites. Therefore, in addition to the well-known reason that interfacial cracks hinder the loading transferring between component materials, the increasing stress concentration is also a significant factor for strength reduction due to interfacial debonding.

With the transverse strengths of the two material systems provided by Refs. [37–40], the load levels when interfacial debonding occurs under 90 ° off-axial tension are calculated from *Eq.* 28. The calculated results (1.1 MPa for the Kevlar fiber reinforced and 40.9 MPa for the glass fiber-reinforced composites) are smaller than two composites' respective transverse tensile strengths (27.7 MPa for the Kevlar fiber-reinforced and 45.3 MPa for the glass fiber-reinforced composites), which means that these two composites will undergo interfacial debonding under transverse tension. Moreover, the critical von Mises stresses, are calculated form *Eq.* 29 in this step (1.2 MPa for the Kevlar fiber reinforced and 59.6 MPa for the glass fiber-reinforced composites).

Given an off-axial tensile load increment, $d\sigma_\theta$, where θ is the off-axial angle, the stress increments $\{d\sigma_{11}^0, d\sigma_{22}^0, d\sigma_{12}^0\}$ can be obtained through a coordinate transformation. Now take the Kevlar fiber reinforced composite with θ of 30 ° as the example to explain how to determine the load level when interfacial cracks appear, which is denoted by $\hat{\sigma}_\theta^0$. First, the homogenized stresses in the matrix are obtained from *Eqs.* 6.2, 6.4, *and* 6.6 as $\sigma_{11}^m = 0.115\sigma_\theta$, $\sigma_{22}^m = 0.234\sigma_\theta$, and $\sigma_{12}^m = -0.32\sigma_\theta$. Multiplying SCFs accordingly, one can get the true stresses in matrix before interfacial debonding as $\overline{\sigma}_{11}^m = 0.115\sigma_\theta$, $\overline{\sigma}_{22}^m = 0.253\sigma_\theta$, and $\overline{\sigma}_{12}^m = -0.374\sigma_\theta$. Then the load level when interfacial debonding occurs in this example can be calculated from *Eq.* 33 as $\hat{\sigma}_{30^0}^0 = 1.11/0.684 = 1.623$ MPa. In the same way, for the Kevlar fiber-reinforced composite under off-axial tension with other off-axial angles, one can obtain $\hat{\sigma}_{45^0}^0 = 1.28$ MPa, $\hat{\sigma}_{60^0}^0 = 1.19$ MPa. Similarly, for the E-glass fiber-reinforced composite, one have $\hat{\sigma}_{30^0}^0 = 103.7$ MPa, $\hat{\sigma}_{45^0}^0 = 66.7$ MPa, $\hat{\sigma}_{60^0}^0 = 50.4$ MPa. The results indicate that interfacial debonding occurs under various loading conditions. The interfacial cracks here are different from manufacturing defects, which already exist before loading. Instead, the interfaces in examples are perfect at first but cracked later when the applied load gets to a certain level. Comparatively speaking, the Kevlar fiber-reinforced material system enters debonding stage much earlier than the E-glass fiber-reinforced composite, indicating that the latter material has got a better interfacial property. This result is consistent with the common observations, which suggests that Kevlar fiber-reinforced polymer composites often undergo interfacial debonding long before the ultimate failure.

After predicting load level of debonding, the stress increments of the matrix are amplified with the corresponding SCFs, respectively, with the final true stresses obtained from *Eqs.* 31 and 32. In this way, the true stresses of matrix in the Kevlar fiber composite with θ = 30 ° are $\overline{\sigma}_{11}^m = 0.115\sigma_\theta$, $\overline{\sigma}_{22}^m = 0.411 + 0.641$ (σ_θ-1.623) and $\overline{\sigma}_{12}^m = -0.374\sigma_\theta$. According to thermoelastic properties provided by Refs. [38,40], the transverse thermal residual stresses in the matrix of the Kevlar fiber-reinforced composite is calculated to be −0.54 MPa, while that of the E-glass fiber/8804 epoxy composite is 8.1 MPa. Together with the true stresses calculated before, the off-axial tensile strength of a composite is calculated from *Eqs.* 34 and 35. In this example, as the matrix failure occurs first, the predicted ultimate 30 ° off-axial tensile strength of the Kevlar fiber composite is obtained from *Eq.* 34 as $\sigma_{30^0}^{u,t} = 80.1$ MPa, which is very close to the measured one, 83.4 MPa [41].

The measurements of two composite materials are provided by Pindera et al. [41] and Mayes et al. [39] and shown in Figs. 5 and 6, respectively. Predictions based on three different considerations have been made, with corresponding results presented in Figs. 5 and 6 for comparison. In the first prediction, the stresses in matrix are regarded as uniform, with no SCF employed. Another is done by taking stress concentration into consideration but ignoring interfacial debonding. Hence, only SCFs based on the assumption of perfect interfacial bonding are used in this prediction. The last one is achieved based on the method proposed in this article, following the steps mentioned in this chapter. All SCFs are applied in the third prediction, including the SCF of composites with cracks on fiber/matrix interface. It can be seen from Figs. 5 and 6 that, as expected, the results given by the prediction without any SCFs applied (the first one) are far away from the experimental data, whereas those come from the prediction with both stress concentration and interfacial debonding considered (the third one) are closest to the measurements. For the second prediction, although the results for the E-glass

 DOI 10.1002/pc

fiber-reinforced composite are accurate enough (Fig. 6), those for the Kevlar fiber-reinforced material system show significant errors (Fig. 5). Moreover, three kinds of predictions give out the same longitudinal tensile strength for each composite, which matches well with measurements. In order to display the results of most off-axial angles more clearly, the predictions with off-axial angles smaller than 10 ° are not included in the figures. On the whole, the method established in this paper can significantly improve the prediction accuracy of the failure strength of composites, especially for material systems with relative weak fiber/matrix interface.

CONCLUSIONS

The SCF of matrix in the composites with interfacial cracks has been derived in this article to quantify the stress concentration after fiber/matrix interface debonding. When considering the effects of interfacial strength on the failure strength of composites, other researchers mainly focus on how interfacial cracks hinder the loading transferring between fibers and matrix, whereas this study pays more attention to the increasing intensity of stress fluctuation in matrix. For instance, the theory put forward in this article also has important practical significance. On one hand, with the standard established in this work, material researchers can obtain more intuitive information about the interface performance in a given material system under arbitrary loads, which is definitely helpful for determining the necessity of interface modification. On the other hand, with the method proposed in this study, one can predict the strength of composites much more conveniently and accurately by using only transverse tensile strength and original constituent information.

ACKNOWLEDGMENT

The authors greatly appreciate the discussion of this work with our colleague, Prof. Y.-D. Xue at Tongji University.

APPENDIX A

TOYA'S SOLUTION

The model developed by Toya [33] was subjected to two orthogonal loads T_∞ and N_∞ at infinity, as shown in Fig. A1. In the following, the equations taken directly from Toya [33] will be labeled with a suffix T. For instance, *Eq.* 2.3T implies that the equation was labeled *Eq.* 2.3 in Toya [33]. The stresses in the matrix read [33]

$$\tilde{\sigma}^{\mathrm{m}}_{33}+\tilde{\sigma}^{\mathrm{m}}_{22}=W(z)+\overline{W}(\bar{z})=2\mathrm{Re}[W(z)], \tag{2.3T}$$

$$\tilde{\sigma}^{\mathrm{m}}_{33}-\tilde{\sigma}^{\mathrm{m}}_{22}+2i\tilde{\sigma}^{\mathrm{m}}_{23}=(\bar{z}-\frac{a^2}{z})W'(z)+\frac{a^2}{z^2}[\overline{W}(\frac{a^2}{z})+W(z)], \tag{AIII.10T}$$

where $W'(z) = dW(z)/dz$. The function $W(z)$ had the following expressions:

$$W(z)=k\left(c_0+c_2/z^2\right)-k\left[(c_0-d_{-1}/k)z+A_1+B_1/z+C_1/z^2\right]\chi(z), \tag{3.7T}$$

$$c_0=G_1+iH_1, \tag{3.28.1T}$$

$$G_1=\frac{0.5(N_\infty+T_\infty)\left[1-(\cos\psi+2\lambda\sin\psi)e^{2\lambda(\pi-\psi)}\right]-0.5(1-k)\left(1+4\lambda^2\right)(N_\infty-T_\infty)\sin^2\psi\cos2\Lambda}{2-k-k(\cos\psi+2\lambda\sin\psi)e^{2\lambda(\pi-\psi)}},$$

$$H_1=\frac{\frac{4\mu_1\omega_\infty}{1+\kappa_1}\left[1+(\cos\psi+2\lambda\sin\psi)e^{2\lambda(\pi-\psi)}\right]+\frac{1}{2}(1-k)\left(1+4\lambda^2\right)(N_\infty-T_\infty)\sin^2\psi\sin2\Lambda}{k+k(\cos\psi+2\lambda\sin\psi)e^{2\lambda(\pi-\psi)}}, \tag{(3.28.2T),(3.28.3T)}$$

$$c_2=a^2(N_\infty-T_\infty)e^{2i\Lambda},\quad A_1=a(\cos\psi+2\lambda\sin\psi)\left(\frac{d_{-1}}{k}-c_0\right), \tag{3.30T),(3.31T}$$

$$B_1=\frac{1-k}{k}a^2(N_\infty-T_\infty)(\cos\psi-2\lambda\sin\psi)\exp[2i\Lambda+2\lambda(\psi-\pi)], \tag{3.32T}$$

$$C_1=-\frac{1-k}{k}a^3(N_\infty-T_\infty)\exp[2i\Lambda+2\lambda(\psi-\pi)], \tag{3.33T}$$

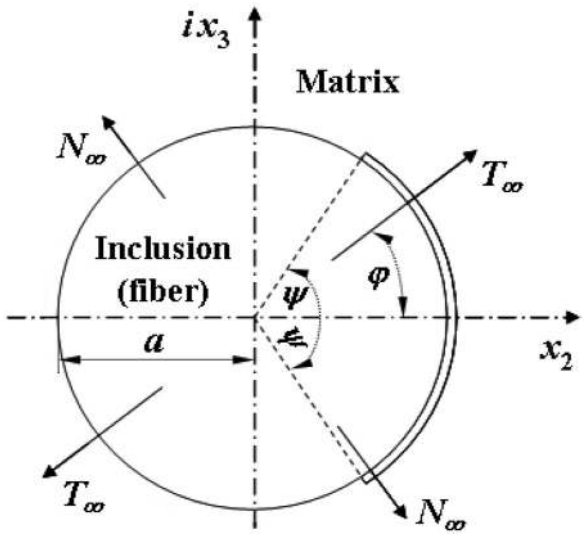

FIG. A1. The model considered by Toya [33].

$$d_{-1}=\frac{N_\infty+T_\infty}{2}+\frac{4\mu_1 i\omega_\infty}{1+\kappa_1},k=\frac{\zeta}{1+\xi}, \quad (3.15.1\text{T},3.9\text{T})$$

$$\lambda=-(ln\xi)/(2\pi),\xi=(\mu_2+\kappa_2\mu_1)/(\mu_1+\kappa_1\mu_2), \quad (3.3\text{T},2.20\text{T})$$

$$\zeta=\mu_1(1+\kappa_2)/(\mu_1+\kappa_1\mu_2),\chi(z)=(z-ae^{i\psi})^{-0.5+i\lambda}(z-ae^{-i\psi})^{-0.5-i\lambda}. \quad (2.21\text{T},3.2\text{T})$$

Moreover, for a plane stress state problem, one has (see p. 326 in Ref. [33])

$$\kappa_1=\frac{4}{1+\nu^{\mathrm{m}}}-1,\kappa_2=\frac{4}{1+\nu^{\mathrm{f}}}-1. \quad (A.1)$$

$\overline{W}(\overline{z})$ represents the conjugate result of $W(z)$. $\overline{W}(z)$ stands for the result of $W(z)$ when all the parameters in $W(z)$ except for z take conjugates. From *Eq.* 3.2T, one gets

$$\overline{\chi}(z)=(z-ae^{-i\psi})^{-0.5-i\lambda}(z-ae^{i\psi})^{-0.5+i\lambda}=\chi(z). \quad (A.2)$$

In the formulas above, ω_∞ represents a rotation at infinity (p. 330 in Ref. [33], and μ_1 and μ_2 denote shear moduli of the matrix and fiber, respectively.

Subtracting *Eq.* 2.3T on both-hand sides from Eqs. AIII.10T, setting $\Lambda = 0$ (Fig. A1), $N_\infty = 0$, $\omega_\infty = 0$, and $T_\infty=\sigma_{22}^0$ to deteriorate Fig. A1 into Fig. 4a, and recognizing that the real part on the left-hand side of the resulting equation is $\tilde{\sigma}_{22}^{\mathrm{m}}$, which should match the real part on the right-hand side, one obtains *Eq.* 19.

APPENDIX B

DERIVATION ON INTEGRATION

Substituting *Eq.* 19.1 into *Eq.* 10 results in the following integration:

$$\hat{K}_{22}^t(\varphi)=\frac{\sigma_{22}^0}{|\vec{\mathrm{R}}_\varphi^b-\vec{\mathrm{R}}_\varphi^a|}\mathrm{Re}\left\{\int_{|\vec{\mathrm{R}}_\varphi^a|}^{|\vec{\mathrm{R}}_\varphi^b|}\frac{\left[\left(\frac{a^2}{z}-\overline{z}\right)M'(z)-\frac{a^2}{z^2}\left[\overline{M}\left(\frac{a^2}{z}\right)+M(z)\right]+2M(z)\right]}{2\left(\sigma_{22}^{\mathrm{m}}\right)_{\mathrm{BM}}}d\left|\vec{R}_\varphi\right|\right\}. \quad (B.1)$$

As $z=e^{i\varphi}R_\varphi$, we have $dR_\varphi=e^{-i\varphi}dz$. The upper and lower bonds in Eq. B.1 change to $b'=be^{i\varphi}=b(\cos\varphi+i\sin\varphi)$ and $a'=ae^{i\varphi}=a(\cos\varphi+i\sin\varphi)$ accordingly. Namely,

$$\hat{K}_{22}^t(\varphi)=\frac{(V_{\mathrm{f}}+A_{22}V_{\mathrm{m}})}{2A_{22}(b-a)}\mathrm{Re}\left\{e^{-i\varphi}\int_{a'}^{b'}\left[\left(\frac{a^2}{z}-\overline{z}\right)M'(z)-\frac{a^2}{z^2}\left[\overline{M}\left(\frac{a^2}{z}\right)+M(z)\right]+2M(z)\right]dz\right\}. \quad (B.2)$$

The integration of Eq. B.2 can be separated into the following ones:

$$\int_{a'}^{b'}\left[\frac{a^2}{z}M'(z)-\frac{a^2}{z^2}M(z)\right]dz=\int_{a'}^{b'}d\left[\frac{a^2}{z}M(z)\right]=\left[\frac{a^2}{z}M(z)\right]_{a'}^{b'} \quad (B.3a)$$
$$=\frac{a^2}{b'}M(b')-\frac{a^2}{a'}M(a')=e^{-i\varphi}\left[\frac{a^2}{b}M(b')-aM(a')\right],$$

$$\int_{a'}^{b'}-\overline{z}M'(z)dz=e^{-2i\varphi}\int_{a'}^{b'}-zM'(z)dz=-e^{-2i\varphi}\left[\{zM(z)\}_{a'}^{b'}-\int_{a'}^{b'}M(z)dz\right]$$
$$=e^{-i\varphi}[aM(a')-bM(b')]+e^{-2i\varphi}\int_{a'}^{b'}M(z)dz, \quad (B.3b)$$

$$\int_{a'}^{b'}\left[-\frac{a^2}{z^2}\overline{M}\left(\frac{a^2}{z}\right)\right]dz=\int_{a'}^{b'}\overline{M}\left(\frac{a^2}{z}\right)d\left(\frac{a^2}{z}\right)=\int_{a^2/a'}^{a^2/b'}\overline{M}(z)dz=\int_{a^2/a'}^{a^2/b'}M(z)dz. \quad (B.3c)$$

It is noted that as the integral range in Eq. B.3c is outside the matrix domain, the integrand $M(z)$ must be changed to that within the fiber region. According to Toya [33], when z takes a value within the fiber region, the function $M(z)$ is still given by *Eq.* 19.2, with the function $\chi(z)$ changed to $\chi_2(z)$, where

$$\chi_2(z)=-\chi(z)/\xi=-\frac{1}{\xi}(z-ae^{i\psi})^{-0.5+i\lambda}(z-ae^{-i\psi})^{-0.5-i\lambda}=\overline{\chi}_2(z). \quad (3.5\text{T})$$

Substituting Eq*s. B.3a–B.3c* into Eq. B.2 results in

$$\begin{aligned}&\int_{a'}^{b'}\left[\left(\frac{a^2}{z}-\overline{z}\right)M'(z)-\frac{a^2}{z^2}\left[\overline{M}\left(\frac{a^2}{z}\right)+M(z)\right]+2M(z)\right]dz\\&=e^{-i\varphi}\left[\frac{a^2}{b}M(b')-aM(a')\right]+e^{-i\varphi}[aM(a')-bM(b')]\\&+e^{-2i\varphi}\int_{a'}^{b'}M(z)dz+\int_{a^2/a'}^{a^2/b'}M(z)dz+2\int_{a'}^{b'}M(z)dz\\&=e^{-i\varphi}M(b')(a^2/b-b)+\int_{a^2/a'}^{a^2/b'}M(z)dz+(2+e^{-2i\varphi})\int_{a'}^{b'}M(z)dz.\end{aligned} \quad (B.4)$$

The remaining work is to integrate $M(z)$. Let us introduce an auxiliary function,

$$R_0(z)=(z-ae^{i\psi})^{0.5+i\lambda}(z-ae^{-i\psi})^{0.5-i\lambda}$$
$$=(z^2+a^2-2za\cos\psi)^{0.5}(z-ae^{i\psi})^{i\lambda}(z-ae^{-i\psi})^{-i\lambda}.$$

It follows that

$$\frac{dR_0}{dz}=0.5(2z-2a\cos\psi)(z^2+a^2-2za\cos\psi)^{-0.5}\left(\frac{z-ae^{i\psi}}{z-ae^{-i\psi}}\right)^{i\lambda}$$
$$+i\lambda(z^2+a^2-2za\cos\psi)^{0.5}\left(\frac{z-ae^{i\psi}}{z-ae^{-i\psi}}\right)^{i\lambda-1}\frac{(z-ae^{-i\psi})-(z-ae^{i\psi})}{(z-ae^{-i\psi})^2}$$
$$=(z-a\cos\psi-2a\lambda\sin\psi)(z-ae^{i\psi})^{-0.5+i\lambda}(z-ae^{-i\psi})^{-0.5-i\lambda}.$$

DOI 10.1002/pc

Therefore,

$$\int [(F-0.5)z+H]\chi(z)dz = \int (F-0.5)[z-a(\cos\psi+2\lambda\sin\psi)]\chi(z)dz$$
$$= (F-0.5)\int \frac{dR_0}{dz}dz = (F-0.5)R_0(z).$$

Similarly, from $\frac{d(R_0/z)}{dz} = -\frac{1}{z^2}R_0(z) + \frac{dR_0}{zdz} = -a^2\left(\frac{1}{z^2} + \frac{2\lambda\ \sin\psi-\cos\psi}{az}\right)\chi(z)$ and $\frac{C}{z} = D(\frac{2\lambda\ \sin\psi-\cos\psi}{az})$, one gets $\int(\frac{C}{z}+\frac{D}{z^2})\chi(z)dz = -D\frac{R_0(z)}{a^2z}$. Finally,

$$\int_{a'}^{b'} M(z)dz = \int_{a'}^{b'}\left(F-\frac{a^2k}{z^2}\right)dz - \int[(F-0.5)z+H]\chi(z)dz - \int\left(\frac{C}{z}+\frac{D}{z^2}\right)\chi(z)dz$$
$$= \left[Fz+\frac{a^2k}{z}-(F-0.5)R_0(z)+D\frac{R_0(z)}{a^2z}\right]_{a'}^{b'} = N(b')-N(a'), \tag{B.5a}$$

$$\int_{a^2/a'}^{a^2/b'} M(z)dz = \left[Fz+\frac{a^2k}{z}+\frac{1}{\xi}\left\{(F-0.5)R_0(z)+D\frac{R_0(z)}{a^2z}\right\}\right]_{a^2/a'}^{a^2/b'}$$
$$= N_1\left(\frac{a^2}{b'}\right)-N_1\left(\frac{a^2}{a'}\right), \tag{B.5b}$$

where $N(z)$ and $N_1(z)$ are given by *Eqs.* 21.2 *and* 21.3, respectively. Substituting *Eqs.* B.5a *and* B.5b into *Eq.* B.4, applying *Eq.* B.2, one can obtain *Eq.* 21.1.

APPENDIX C

DETERMINATION OF A CRACK ANGLE

Using polar coordinates (ρ, θ), Toya [33] obtained the relative displacements of the two faces of the crack under uniaxial tension (Fig. 4a):

$$u_\rho + iu_\theta = -\frac{1}{2}A_2\sigma_{22}^0 a\left\{G_0 - \frac{1}{k} - \frac{2(1-k)a}{kt}\exp[2\lambda(\psi-\pi)]\right\}\frac{R_0(t)}{t}, \tag{3.54T}$$

$$A_2 = \frac{k}{4}\left(\frac{1+\kappa_1}{\mu_1}+\frac{1+\kappa_2}{\mu_2}\right). \tag{3.39T}$$

In *Eq.* 3.54T, $t = ae^{i\varphi}$ is a point on the interface (p. 328) in Ref. [33], G_0 and $R(e^{i\Phi}) = R_0(t)/t$ are given in *Eqs.* 24.1 *and* 24.2, respectively. The crack angle Ψ must fulfill

$$u_\rho(t) = u_\rho(ae^{i\varphi})|_{\varphi=\psi} = 0. \tag{C.1}$$

However, *Eq.* 24.2 implies that Eq. C.1 is fulfilled automatically, thus no Ψ can be solved from it. On the other hand, both England [42] and Toya [33] pointed out that the relative displacement at another point of the interface with a smaller central angle, $2\varphi = 2(\Psi - \gamma)$, was also zero. In other words, Eq. C.1 should be replaced by *Eq.* 23.

To simplify *Eq.* 23, let us consider the norm and phase angle of the variable$[\exp(i(\varphi))-e^{i\psi}]$, which are given, respectively, by

$$|\exp(i(\varphi))-e^{i\psi}| = |\cos\varphi-\cos\psi+i(\sin\varphi=\sin\psi)|$$
$$= \sqrt{(\cos\varphi-\cos\psi)^2+(\sin\varphi-\sin\psi)^2} \tag{C.2a}$$
$$= \sqrt{2-2[1-2\sin^2(0.5(\psi-\varphi))]} = 2\sin(0.5|\psi-\varphi|),$$

$$\mathrm{Arg}[\exp(i\varphi)-e^{i\psi}] = \tan^{-1}\left(\frac{\sin\varphi-\sin\psi}{\cos\varphi-\cos\psi}\right) = \tan^{-1}\left(\frac{\sin\varphi-\sin(\varphi+\gamma)}{\cos\varphi-\cos(\varphi+\gamma)}\right)$$
$$= \tan^{-1}\left(\frac{\sin\varphi\ \sin(0.5\gamma)-\cos\varphi\ \cos(0.5\gamma)}{\cos\varphi\ \sin(0.5\gamma)+\sin\varphi\ \cos(0.5\gamma)}\right) = \tan^{-1}\left(\frac{-\cos(\varphi+0.5\gamma)}{\sin(\varphi+0.5\gamma)}\right)$$
$$= -(0.5\pi-\varphi-0.5\gamma) = \varphi+0.5\gamma-0.5\pi. \tag{C.2b}$$

Similarly,

$$|\exp(i(\varphi))-e^{-i\psi}| = |\cos\varphi-\cos\psi+i(\sin\varphi+\sin\psi)|$$
$$= \sqrt{2-2(\cos\varphi\ \cos\psi-\sin\varphi\ \sin\psi)} = \sqrt{2-2\cos(\psi+\varphi)} \tag{C.3a}$$
$$= \sqrt{2-2[1-2\sin^2(0.5(\psi+\varphi))]} = 2\sin(0.5(\psi+\varphi)),$$

$$\mathrm{Arg}[\exp(i\varphi)-e^{i\psi}] = \tan^{-1}\left(\frac{\sin\varphi+\sin\psi}{\cos\varphi-\cos\psi}\right) = \tan^{-1}\left(\frac{\sin\varphi+\sin(\varphi+\gamma)}{\cos\varphi-\cos(\varphi+\gamma)}\right)$$
$$= \tan^{-1}\left(\frac{2\sin\varphi\ \cos^2(0.5\gamma)+2\cos\varphi\ \sin(0.5\gamma)\cos(0.5\gamma)}{2\cos\varphi\ \sin^2(0.5\gamma)+2\sin\varphi\ \sin(0.5\gamma)\cos(0.5\gamma)}\right)$$
$$= \tan^{-1}\left(\frac{\cos(0.5\gamma)}{\sin(0.5\gamma)}\right) = 0.5\pi-0.5\gamma. \tag{C.3b}$$

Hence, $R(\exp(i\varphi)) = [\exp(i(\varphi))-e^{i\psi}]^{0.5+i\lambda}[\exp(i(\varphi))-e^{-i\psi}]^{0.5-i\lambda}\exp(-i(\varphi)) = [2\sin(0.5|\psi-\varphi|)e^{(i(\varphi+0.5\gamma-0.5\pi))}]^{0.5+i\lambda}\times[2\sin((\psi+\varphi)/2)e^{(i(0.5\pi-0.5\gamma))}]^{0.5-i\lambda}e^{(-i\varphi)}$.

As $r^{i\lambda} = (e^{\ln r})^{i\lambda} = e^{i(\lambda\ln r)}$, one further obtains

$$R(\exp(i\varphi)) = \exp(-i\varphi)[4\sin((\psi-\varphi)/2)\sin((\psi+\varphi)/2)]^{0.5}$$
$$\exp(i\lambda\ln(2\sin((\psi-\varphi)/2)))\times$$
$$\exp(-i\lambda\ln(2\sin((\psi-\varphi)/2)))[\exp(i(\varphi+0.5\gamma-0.5\pi))]^{0.5+i\lambda}$$
$$[\exp(i(0.5\pi-0.5\gamma))]^{0.5-i\lambda}$$
$$= 2[\sin(0.5)|\psi-\varphi|\sin((\psi+\varphi)/2)]^{0.5}\exp(i\lambda\ln(\sin((\psi-\varphi)/2)/$$
$$\sin((\psi+\varphi)/2)))\times$$
$$\exp[-\lambda(\varphi+0.5\gamma-0.5\pi)+\lambda(0.5\pi-0.5\gamma)]\exp\{i[-0.5\varphi]\}$$
$$= 2[\sin(0.5|\psi-\varphi|)\sin((\psi+\varphi)/2)]^{0.5}\exp[\lambda(\pi-\psi)]\times$$
$$\exp[i[\lambda\ln(\sin((\psi-\varphi)/2)/\sin((\psi+\varphi)/2))-0.5\varphi]\}. \tag{C.4}$$

For any two variables A and B, one has $AB = |A|\exp(i\varphi_A)|B|\exp(i\varphi_B) = |A||B|\exp[i(\varphi_A+\varphi_B)]$. In other words, $Re(AB) = 0$ is equivalent to $\varphi_A + \varphi_B = \pm 0.5\pi$, where φ_A and φ_B are the phase angles of A and B,

respectively. A solution to *Eq.* 23 is equivalent to that to the following equation:

$$Arg\left[G_0-\frac{1}{k}-\frac{2(1-k)}{k\exp(i\varphi)}\exp(2\lambda(\psi-\pi))\right]+Arg[R(\exp(-i\varphi))]=\pm\frac{\pi}{2}$$

Substituting *Eq.* C.4 into the last equation leads to

$$\begin{aligned}&\tan^{-1}\left(\frac{2(1-k)\exp[2\lambda(\psi-\pi)]\sin\varphi}{kG_0-1-2(1-k)\exp[2\lambda(\psi-\pi)]\cos\varphi}\right)\\&+\lambda\ln\left(\frac{\sin[0.5(\psi-\varphi)]}{\sin[0.5(\psi+\varphi)]}\right)-\frac{\varphi}{2}=\pm\frac{\pi}{2},\\&or,\ \tan^{-1}\left(\frac{2(1-k)\xi\exp(2\lambda\psi)\sin\varphi}{kG_0-1-2(1-k)\xi\exp(2\lambda\psi)\cos\varphi}\right)\\&+\lambda\ln\left(\frac{\sin[0.5(\psi-\varphi)]}{\sin[0.5(\psi+\varphi)]}\right)-\frac{\varphi}{2}=\pm\frac{\pi}{2},\end{aligned}\qquad(C.5a,C.5b)$$

in which $\varphi = \Psi - \gamma$. Let us consider two different cases. When $\xi \le 1$, we have

$$k=\frac{\mu_1(1+\kappa_2)}{(1+\nu)(\mu_1+\kappa_1\mu_2)}=\frac{\mu_1+\kappa_2\mu_1}{\mu_1+\kappa_2\mu_1+\mu_2+\kappa_1\mu_2}<1,\lambda=-\ln(\xi)/(2\pi)\ge 0,$$
$$2(1-k)\exp[2\lambda(\psi-\pi)]>0\ and\ k^{-1}>1>0.5(1+4\lambda^2)\sin^2\psi.$$

Hence, $kG_0=\frac{1-(\cos\psi+2\lambda\ \sin\psi)\exp[2\lambda(\pi-\psi)]+(1-k)(1+4\lambda^2)\sin^2\psi}{2/k-1-(\cos\psi+2\lambda\ \sin\psi)\exp[2\lambda(\pi-\psi)]}<1.$

Noticing that both sin φ and cos φ are > 0, it follows that

$$\tan^{-1}\left(\frac{2(1-k)\xi\exp(2\lambda\psi)\sin(\varphi)}{kG_0-1-2(1-k)\xi\exp(2\lambda\psi)\cos(\varphi)}\right)<0.\qquad(C.6)$$

$$\text{At the same time, }\lambda\ln\left(\frac{\sin(0.5(\psi-\varphi))}{\sin(0.5(\psi+\varphi))}\right)\le 0.\qquad(C.7)$$

Equations C.6 *and* C.7 imply that one should choose -0.5π on the right-hand side of Eq. C.5. Equation C.5b is further simplified to

$$\lambda\ln\left(\frac{\sin[0.5(\psi-\varphi)]}{\sin[0.5(\psi+\varphi)]}\right)=\frac{\varphi}{2}-\frac{\pi}{2}-\tan^{-1}\left(\frac{2(1-k)\xi\exp(2\lambda\psi)\sin\varphi}{kG_0-1-2(1-k)\xi\exp(2\lambda\psi)\cos\varphi}\right),$$

with

$$\frac{\sin[0.5(\psi-\varphi)]}{\sin[0.5(\psi+\varphi)]}=\exp\left(\frac{1}{\lambda}\left[\frac{\varphi}{2}+\tan^{-1}\left(\frac{kG_0-1-2(1-k)\xi\exp(2\lambda\psi)\cos(\psi-\gamma)}{2(1-k)\xi\exp(2\lambda\psi)\sin(\psi-\gamma)}\right)\right]\right).$$

In other words,

$$\exp\left(\frac{1}{\lambda}\left[\frac{\psi-\gamma}{2}+\tan^{-1}\left(\frac{kG_0-1-2(1-k)\xi\exp(2\lambda\psi)\cos(\psi-\gamma)}{2(1-k)\xi\exp(2\lambda\psi)\sin(\psi-\gamma)}\right)\right]\right)-\frac{\gamma}{2\sin(\psi)}=0.\qquad(C.8)$$

To derive the last equation, the conditions that sin $(0.5\gamma) \approx 0.5\gamma$, $\sin(\Psi - 0.5\gamma) \approx \sin(\Psi)$ and $-0.5\pi - \tan^{-1}(1/\omega) = \tan^{-1}(\omega)$ were taken into account. As a geometrical interpretation of Eq. C.8 is that the relative displacement in the radial direction between the fiber and matrix faces attains the minimum, the first-order derivative of the function $\gamma f(\gamma)$ (because of $\gamma > 0$) must be zero at γ. Namely,

$$\frac{d(\gamma f(\gamma))}{d\gamma}=\left\{\gamma\exp\left[\frac{1}{\lambda}\left(\tan^{-1}(J_1/J_2)+\frac{\psi}{2}\right)\right]\frac{1}{\lambda}\left[\frac{J_3J_2}{J_1^2+J_2^2}-\frac{1}{2}\right]+\exp\left[\frac{1}{\lambda}\left(\tan^{-1}(J_1/J_2)+\frac{\psi}{2}\right)\right]-\frac{\gamma}{\sin(\psi)}\right\}=0,\qquad(C.9)$$

where J_1, J_2, and J_3 are defined by *Eqs.* 25.3-25.5. It is noted that as γ is much smaller than Ψ, the variable $\Psi - \gamma$ in all the functions in *Eq.* C.9 and *Eqs.* 25.3-25.5 has been replaced by Ψ. From *Eq.* C.9, one obtains

$$\gamma=\frac{\lambda\exp\left[\frac{1}{\lambda}\left(\tan^{-1}(J_1/J_2)+\frac{\psi}{2}\right)\right]}{\exp\left[\frac{1}{\lambda}\left(\tan^{-1}(J_1/J_2)+\frac{\psi}{2}\right)\right]\left[\frac{1}{2}-\frac{J_3J_2}{J_1^2+J_2^2}\right]+\frac{\lambda}{\sin(\psi)}}.\qquad(C.10)$$

Equation 25.1 is resulted from Eq. C.10 as $\lambda \ll \exp\left\{\frac{1}{2\lambda}[2\tan^{-1}(J_1/J_2)+\psi]\right\}\sin(\psi)$.

If $\xi > 1$, we have $\lambda = -\ln(\xi)/(2\pi) < 0$. In such a case, a minimum value of the function $\gamma f(\gamma)$ is no longer able to be assumed. Instead, we request $f(\gamma)$ to attain the minimum. From the latter condition, one has

$$\frac{f'(\gamma)}{\sin(\psi)}=\frac{1}{\gamma}\exp\left(\frac{1}{\lambda}\left[\frac{\psi-\gamma}{2}+\tan^{-1}(J_1/J_2)\right]\right)\frac{1}{\lambda}\left(-\frac{1}{2}+\frac{J_3J_2}{J_1^2+J_2^2}\right)-\frac{1}{\gamma^2}\exp\left(\frac{1}{\lambda}\left[\frac{\psi-\gamma}{2}+\tan^{-1}(J_1/J_2)\right]\right)=0,$$

which gives out *Eq.* 25.2.

REFERENCES

1. Z.R. Yue, W. Jiang, L. Wang, S.D. Gardner, and C. U. Pittman, *Carbon*, **37**, 1785 (1999).
2. B. Abeles, R.B. Hall, M. Zhou, *U.S. Patent*, **5846**, 641 (1998).
3. Y. Xie, C.A.S. Hill, Z. Xiao, H. Militz, and C. Mai, *Compos. A Appl. Sci. Manuf.*, **41**, 806 (2010).
4. M. Peroglio, L. Gremillard, J. Chevalier, L. Chazeau, C. Gauthier, and T. Hamaide, *J. Eur. Ceram. Soc.*, **27**, 2679 (2007).
5. L. Liu, Y.D. Huang, Z.Q. Zhang, Z.X. Jiang, and L.N. Wu, *Appl. Surf. Sci.*, **254**, 2594 (2008).
6. Z. Xu, Y. Huang, C. Zhang, L. Liu, Y. Zhang, and L. Wang, *Compos. Sci. Tech.*, **67**, 3261 (2007).
7. J.K. Kim and Y.W. Mai, Engineered Interfaces in Fiber Reinforced Composites, Elsevier, Amsterdam (1998).

8. J. Llorca, C. Gonzalez, J.M. Molina-Aldareguía, J. Segurado, R. Seltzer, F. Sket, M. Rodríguez, S. Sadaba, R. Muñoz, and L.P. Canal, *Adv. Mater.*, **23**, 5130 (2011).
9. X.F. Zhou, H.D. Wagner, and S.R. Nutt, *Compos. A Appl. Sci. Manuf.*, **32**, 1543 (2001).
10. M. Nishikawa, T. Okabe, K. Hemmi, and N. Takeda, *Int. J. Solids Struct.*, **45**, 4098 (2008).
11. H. Ho, and L.T. Drzal, *Compos. A Appl. Sci. Manuf.*, **27**, 961 (1996).
12. G.P. Tandon, R.Y. Kim, S.G. Warrier, and B.S. Majumdar, *Compos. B Eng.*, **30**, 115 (1999).
13. M.R. Piggott, *Compos. Sci. Tech.*, **57**, 965 (1997).
14. M.S. Madhukar, and L.T. Drzal, *J. Compos. Mater.*, **25**, 932 (1991).
15. P.J. Herrera-Franco, and L.T. Drzal, *Composites*, **23**, 2 (1992).
16. D.M. Blackketter, D. Upadhyaya, and T.R. King, *Polym. Compos.*, **14**, 437 (1993).
17. C.T. Sun, J.L. Chen, G.T. Sha, and W.E. Koop, *J. Compos. Mater.*, **24**, 1029 (1990).
18. T. Hobbiebrunken, M. Hojo, T. Adachi, C.D. Jong, and B. Fiedler, *Compos. A Appl. Sci. Manuf.*, **37**, 2248 (2006).
19. G. Qi, S. Du, B. Zhang, Z. Tang, and Y. Yu, *Compos. Sci. Tech.*, **105**, 1 (2014).
20. Z.M. Huang, and L. Liu, *Int. J. Mech. Sci.*, **79**, 105 (2014).
21. Z.M. Huang, and L.M. Xin, *Acta Mech. Sin.*, **33**, 120 (2017).
22. Z.M. Huang, and Y.X. Zhou, Strength of Fibrous Composites, Zhejiang University Press & Springer, Hangzhou, New York (2011).
23. S. Ryan, M. Wicklein, A. Mouritz, W. Riedel, F. Schäfer, and K. Thoma, *Int. J. Impact Eng.*, **36**, 899 (2009).
24. A. Shaw, S. Sriramula, P.D. Gosling, and M.K. Chryssanthopoulos, *Compos. B Eng.*, **41**, 446 (2010).
25. A. Hallal, F. Fardoun, and R. Younes, *Adv. Comp. Mater.*, **324**, 189 (2011).
26. P.D. Soden, M.J. Hinton, and A.S. Kaddour, *Compos. Sci. Tech.*, **58**, 1011 (1998).
27. J.D. Eshelby, *Proc. R. Soc. A*, **241**, 376 (1957).
28. Y. Benveniste, G.J. Dvorak, and T. Chen, *Mech. Mater.*, **7**, 305 (1989).
29. R. Talreja, *Compos. Sci. Tech.*, **105**, 190 (2014).
30. H.N. Wei, A.G. Salvi, and A.M. Waas, *Compos. Sci. Tech.*, **70**, 1126 (2010).
31. D.J. Mortell, D.A. Tanner, and C.T. McCarthy, *Compos. Sci. Tech.*, **105**, 118 (2014).
32. J. Koyanagi, S. Ogihara, H. Nakatani, T. Okabe, and S. Yoneyama, *Adv. Comp. Mater.*, **23**, 551 (2014).
33. M. Toya, *J. Mech. Phys. Solids*, **22**, 325 (1974).
34. M.R. Wisnom, *J. Compos. Mater.*, **24**, 707 (1990).
35. F. París, E. Correa, and J. Cañas, *Compos. Sci. Tech.*, **63**, 1041 (2003).
36. Z.M. Huang, *J. Compos. Mater.*, **35**, 281 (2001). Kavlar 23.4,-0.5 8804 12.7,8.1
37. J. Aboudi, *Compos. Sci. Tech.*, **33**, 79 (1988).
38. S. Rojstaczer, D. Cohn, and G. Marom, *J. Mater. Sci. Lett.*, **4**, 1233 (1985).
39. S. Mayes, C. Andrew, and J. Hansen, *Mech. Adv. Mat. Struct.*, **8**, 249 (2001).
40. P. Suppakul, and S. Bandyopadhyay, *Compos. Sci. Tech.*, **62**, 709 (2002).
41. M.-J. Pindera, Z. Gurdal, C.T. Herakovich, J.S. Hidde, and J. M. Starbuck, *J. Reinf. Plast. Comp.*, **8**, 410 (1989).
42. A.H. England, *J. Appl. Mech.*, **33**, 637 (1966).